Electroreflectance and ellipsometry of silicon from 3 to 6 eV

A. Daunois
Laboratoire de Spectroscopie et d'Optique du Corps Solide, Université Louis Pasteur, 67000 Strasbourg, France and Bell Laboratories, Murray Hill, New Jersey 07974*

D. E. Aspnes
Bell Laboratories, Murray Hill, New Jersey 07974

(Received 21 December 1977)

Using a five-band model, we calculate the effect of the k-linear intravalence band coupling term on dielectric function, third derivative, and low-field electroreflectance (ER) line shapes for Si. The k-linear term, which was recently shown by Cardona strongly to affect transverse-interband reduced-mass values on the $\langle 111\rangle$ symmetry axes, acts to increase the oscillator strength of the upper valence (v)–lower conduction (c) band transitions at the expense of that of the lower spin-orbit split valence bands and c. Using reasonable values of parameters, we show that the $E_1+\Delta_1$ transition in ER is weakened to the point where it appears only as a subsidiary oscillation, qualitatively in agreement with experiment. Other experimental evidence for the k-linear term includes the absence of a low-field limit for the E_1 structure, which is believed to arise from the strong nonparabolicity of the valence bands near the $\langle 111\rangle$ axes. All E_1 data, including in addition ER polarization anisotropies and a comparison between ER and numerically differentiated third-derivative spectra, are consistent with a three-dimensional M_1 critical point (or point set) at or near L and a three-dimensional M_0 critical point at Γ. A third, non-Λ critical-point structure is observed slightly above the M_1 structure, too close to be resolved. Both theory and experiment yield no evidence for the anomalously small transverse reduced mass reported by Grover and Handler: the E_1, not the $E_1+\Delta_1$, transition dominates, and as may be expected from the nonparabolicity the "apparent" mass obtained from the ratio of the magnitudes of the ER and third-derivative spectra, both theoretical and experimental, is larger than that calculated without intravalence coupling. Threshold energies are obtained for all observed critical points. For the E_2 region, a numerically differentiated second-derivative line shape gives the best fit to the ER spectrum for reasons which are not clear.

I. INTRODUCTION AND SUMMARY

A number of different modulation techniques have been developed to investigate the optical spectra of solids.[1] Of these techniques, low-field electroreflectance[2-7] (ER) is particularly well adapted for high-resolution optical spectroscopy because the line shapes obtained are related to the third derivative of the unperturbed dielectric function.

The higher-interband optical structure of silicon has been studied by essentially all modulation techniques,[8-10] including low-field ER.[11-16] We mention in particular the flatband electrolyte work of Grover and Handler[13] (GH), who investigated ER spectra at room temperature from 3.1 to 3.6 eV, and the low-temperature Schottky barrier low-field ER results of Kondo and Moritani (KM) and co-workers,[14-16] who studied also the piezoelectroreflectance response from 3.0 to 5.0 eV of crystals stressed uniaxially along high-symmetry directions.

The most attention has been given to the complicated 3.4-eV structure. Theory[17-23] shows that it arises primarily from transitions along the $\langle 111\rangle$ directions of the Brillouin zone, but that it may also contain contributions from the zone center and possibly also from $\langle 100\rangle$ regions as well. In the more recent low-field ER work, GH[13] interpreted their data in terms of a two-dimensional (2D) M_0 critical point along Λ. Their results were remarkable in that the reduced mass obtained as a best-fit adjustable parameter was found to be $0.022\,m_e$, about one-fifth of the value, $0.11m_e$, expected from simple $\vec{k}\cdot\vec{p}$ theory.[24] GH also had to assume the existence of a weak M_1 critical point at a lower energy than that of the main 2D M_0 structure to obtain the best line-shape agreement, but they pointed out the basic inconsistency of such a critical-point ordering. KM[15] assigned the main structure to a 3D M_1 critical point with $|\mu_L| \gg \mu_T$, qualitatively similar to and consistent with the interpretation of GH, and assigned the lower, weaker structure to a 3D M_0 critical point at Γ.

While it would seem that the interpretation of Si optical spectra is well in hand, two recent developments have occurred that can in principle provide new insight into these spectra. The first of these is Cardona's evaluation, for Si,[25] of the effect of the k-linear intervalence-band coupling term.[26] This term, although always present in multiple-band calculations, is normally neglected in two- or three-band approximations because its influence is small unless the spin-orbit splitting is

small, and because it affects the band structure only in directions perpendicular to the ⟨111⟩ symmetry directions which are usually not plotted. Cardona showed that this term was important in Si owing to the small ($\Delta_{SO} \cong 0.029$ eV $\cong \frac{2}{3} \times 0.044$ eV)[27] spin-orbit splitting of the valence bands of Si along the ⟨111⟩ directions. In fact, Cardona showed that the anomalously small mass observed by GH was just that of the spin-orbit-split (SO) valence to conduction (c) band transitions at $k_\perp = 0$, averaged along the Λ axis. The second development is high-precision scanning ellipsometry,[28,29] from which one can obtain dielectric-function data which are sufficiently precise for multiple differentiation, and therefore sufficiently precise for direct comparison to ER spectra according to the third-derivative relation obtained from low-field theory.[3,30]

In this paper, we investigate the effect of the k-linear terms on the interpretation of the low-field ER spectra, and also the comparison of low-field ER spectra to ellipsometric data. Section II deals with the analysis of a five-band model evaluated with Si parameters and k-linear coupling to determine how the k-linear terms may be expected to affect ϵ_2, ER, and third-derivative spectra. Experimental aspects are discussed in Sec. III. ER results are analyzed and compared to ellipsometric data in Sec. IV, and the critical-point values summarized in Table I. The principal results of Sec. II are as follows:

(i) A five-band model calculation shows that the k-linear coupling induces a threefold symmetric nonparabolic distortion into the SO and v bands, which for sufficiently large k-linear coupling pushes the v-c critical point off the ⟨111⟩ symmetry

TABLE I. Experimental and theoretical critical-point energies for silicon (eV).

		Experimental			Theoretical				
Transition	Designation and type	10 K	80 K	293 K	Herman *et al.*[a]	Kane[b]	Saravia[c] and Brust	Saravia[d]	Chelikowsky and Cohen[e]
$\Gamma^v_{25'} \rightarrow \Gamma^c_{15}$	E_0'	3.365 ± 0.01[f]	3.37[g]	3.330 ± 0.01[f]	2.7	3.2	3.39	3.2	3.42
	M_0	3.4[h]	3.36[i]	3.294[k] 3.281[j]		2.98			
	E_1	3.46 ± 0.015[f]	3.485[g]	3.40 ± 0.015[f]		2.9	3.37		
$\Lambda^v_3 \rightarrow \Lambda^c_1$	E_1			3.412[k]	3.4	3.01	3.54	3.34	3.46
	M_0, M_1	3.45[h]	3.41[i]	3.36[j]					
$\Gamma^v_{25'}(\Gamma_{8'}) \rightarrow \Gamma^c_2$,	$E_0, E_0 + \Delta_0$	4.18[f]							
		4.185[l]			4.2	3.3		4.2	4.10
$\Gamma^v_{25'}(\Gamma_{7'}) \rightarrow \Gamma^c_{2'}$	M_0	4.225[f]				3.61			
		4.229[l]							
$\Sigma_v \rightarrow \Sigma_c$	E_2	4.33 ± 0.015[f]	4.26[i]						4.47
		4.6 ± 0.02[f]	4.46[i]		4.3	4.1			
	M_1, M_2?	4.44[h]	4.336[m]						4.6
		4.60[h]	4.459[m] 4.598[m]						
$\Lambda^v_3 \rightarrow \Lambda^c_3$	E_1'	5.45[f]				5.3	5.22	5.05	5.57
	M_1, M_2 ?	5.5[h]							

[a] F. Herman, R. L. Kortum, C. D. Kuglin, and R. A. Short, Ref. 19.
[b] E. O. Kane, Ref. 20.
[c] L. R. Saravia and D. Brust, Ref. 21.
[d] L. R. Saravia, Ref. 22.
[e] J. R. Chelikowsky and M. L. Cohen, Ref. 23.
[f] This work.
[g] R. A. Forman, D. E. Aspnes, and M. Cardona, Ref. 11.
[h] R. R. L. Zucca and Y. R. Shen, Ref. 8.
[i] R. Braunstein and M. Welkowsky, Ref. 9.
[j] J. W. Grover and P. Handler, Ref. 13.
[k] K. Kondo and A. Moritani, Ref. 15.
[l] D. E. Aspnes and A. A. Studna, Ref. 12.
[m] K. Kondo and A. Moritani, Ref. 16.

axes to form three sets of critical points in directions away from the nearest cube edges. The SO-c critical points remain at $k_\perp = 0$.

(ii) The nonparabolic distortion greatly increases the density of states of the E_1 transitions at the expense of that of the $E_1 + \Delta_1$ transitions and produces a 25% increase of the total ϵ_2 curve compared to that calculated without the k-linear term. The effect is greatly enhanced in the calculated third joint-density-of-states (JDOS) derivation spectrum, where an intravalence-band momentum matrix element $\Pi_v = 0.2\hbar G_0$, where $G_0 = 2\pi/a_0$ and[31] $a_0 = 10.263 a_B$ is the lattice constant of Si, produces an apparent v-c structure about 14 times larger than the apparent SO-c structure in the calculated third-derivative spectrum. (The value $\Pi_v \cong 0.2\hbar G_0$ is that expected over the middle third of the Λ symmetry axes in the Brillouin zone.[25]) By contrast, for $\Pi_v = 0$ (no k-linear term) they are about equal. Thus we expect higher-derivative spectra to arise from the v-c transitions, not from SO-c transitions.

(iii) Despite the tendency of low-mass critical points to be enhanced by the acceleration mechanism of low-field ER, the approximate five-band model calculation shows that the v-c structure still dominates the SO-c structure. The v-c to SO-c structure ratio for $\Pi_v = 0.2\hbar G_0$ is 5.2, compared to 0.71 for $\Pi_v = 0$. The SO-c structure in fact looks like a subsidiary oscillation, in qualitative agreement with data.

(iv) By comparing relative amplitudes of the theoretical ER and third-derivative spectra for an assumed broadening of $\Gamma = 30$ meV, we find an apparent transverse interband mass of $+0.107 m_e$ for the v-c transition for $\Pi_v = 0.2\hbar G_0$, far different from the $k_\perp = 0$ value of $-0.10 m_e$. Thus the band nonparabolicity is so extreme that the $k_\perp = 0$ mass values are almost irrelevant.

The principal results of Sec. IV are as follows: (i) Field and polarization dependences are used to establish the presence of a third critical point in the E_1 spectrum. This critical point is nearly degenerate with the dominant M_1 singularity. This critical point is not of $\langle 111 \rangle$ symmetry and is expected to affect the polarization anisotropy observed for the dominant E_1 structure.

(ii) The dominant E_1 structure appears to have no low-field limit, by contrast to the rest of the E_1 spectrum and to the results reported by KM[15] using larger fields. We interpret this as arising from strong nonparabolicity effects which occur from the k-linear term and the small spin-orbit splitting.

(iii) Polarization anisotropy suggests that the dominant E_1 structure arises from an M_1 critical point, in agreement with the conclusions of KM.[15] The larger transverse mass of the v-c structure relative to that of the SO-c structure, obtained from the model calculation, leads to a natural explanation of the small shift to lower energy of the ER spectrum obtained with [001] polarization relative to that obtained with $[1\bar{1}0]$ polarization.

(iv) If the dominant E_1 structure is assumed to have a long low-energy tail of the type observed in[32] Ge and GaAs,[6] an M_0 critical point origin for the lower-energy E_0' structure follows directly. Because the low-energy tail cannot be described by simple parabolic models, such fits to complete spectra should be treated cautiously.

(v) The third JDOS derivative of the ellipsometrically measured ϵ_1 spectrum for the E_1 transitions agrees with the $\Delta\epsilon_1$ spectrum calculated from ER data if a 60° phase shift is included. Thus the third-derivative relationship for E_1 is essentially satisfied for Si. But the transverse mass obtained by comparing amplitudes is a factor of 4 too large, showing that Coulomb effects are important.[33-35] Further support for Coulomb effects comes from the fact that the measured ϵ_2 spectrum is about 1.5 times larger than the model spectrum and that it peaks strongly at threshold at 10 K. Here, the capability to do numerical differentiation is significant because in a 2D situation the magnitude of the ER spectrum is independent of the value of the transverse mass.[3]

(vi) The two E_2 transitions show large but different polarization anisotropies, suggesting M_1 or M_2 types of critical points with origins at different points of the Brillouin zone.

(vii) The ER spectra of the E_2 transitions are fit better with a second JDOS derivative than with a third JDOS derivative. No obvious reason for this behavior is known, although it probably arises from the same extreme phase shift of calculated third JDOS spectra relative to low-field ER spectra that is seen for E_2 structures in other materials as well.

(viii) The most recent band structure calculations are essentially supported, with the Chelikowsky-Cohen[23] calculation being somewhat better than that of Saravia.[22] We find no support either theoretically or experimentally for the small E_1 transverse mass reported by GH.[13]

II. THEORY

In this section, we evaluate a five-band k-linear Hamiltonian that describes approximately the energy band structure of the $\Delta_{4,5}$, Δ_6 upper valence bands and the Δ_6 singlet and the $\Delta_{4,5}$, Δ_6 lower conduction bands of Si along the $\langle 111 \rangle$ directions. Our purpose is to obtain a qualitative feeling for the experimental results. We suppose for simplicity

cylindrical symmetry along each of the eight ⟨111⟩ directions, each of which is assumed to have length of 80% of that from Γ to L, or $K_z = 0.8(\sqrt{3}/2)\hbar G_0$.

Let $\vec{k} = k\hat{\rho}$ be the wave vector perpendicular to the [111] symmetry axis in the vicinity of the [111] symmetry axis. Then the energies of the upper valence and lowest conduction bands are given approximately by the solutions W_j of the three-band Hamiltonian,

$$\det \begin{vmatrix} E_c^0(k) - W_j & \frac{\hbar k P}{\sqrt{2}m_e} e^{i\phi} & \frac{\hbar k P}{\sqrt{2}m_e} e^{-i\phi} \\ \frac{\hbar k P}{\sqrt{2}m_e} e^{-i\phi} & E_v^0(k) - W_j & -i\frac{\hbar k \Pi_v}{m_e} e^{i\phi} \\ \frac{\hbar k P}{\sqrt{2}m_e} e^{i\phi} & i\frac{\hbar k \Pi_v}{m_e} e^{-i\phi} & E_{SO}^0(k) - W_j \end{vmatrix} = 0 . \tag{1}$$

where the subscripts c, v, and SO refer to the Λ_1 conduction, Λ_6 (upper) valence, and $\Lambda_{4,5}$ (lower, spin-orbit-split) valence bands, respectively. In Eq. (1), P and Π_v are defined as usual as

$$P = \langle \bar{X} | \bar{P}_x | c \rangle = \langle \bar{Y} | \bar{P}_y | c \rangle , \tag{2a}$$

$$\Pi_v = \langle \bar{X} | \bar{P}_x | \bar{Y} \rangle = \langle \bar{X} | \bar{P}_y | \bar{X} \rangle = -\langle \bar{Y} | \bar{P}_y | \bar{Y} \rangle , \tag{2b}$$

and ϕ is defined as

$$\bar{k}_x = k\cos\phi, \ \bar{k}_y = k\sin\phi . \tag{2c}$$

In Eqs. (2), the overbar denotes quantities referred to the rotated unit vector set

$$\hat{\bar{z}} = (\hat{x} + \hat{y} + \hat{z})/\sqrt{3}, \tag{3a}$$

$$\hat{\bar{x}} = (\hat{x} - \hat{y})/\sqrt{2}, \tag{3b}$$

$$\hat{\bar{y}} = (\hat{x} + \hat{y} - 2\hat{z})/\sqrt{6}, \tag{3c}$$

c is the Λ_1 conduction band, and $\bar{X}$ and $\bar{Y}$ are an orthogonal basis representation of the Λ_3 upper valence band in the absence of spin-orbit splitting. The quantity

$$Q = \langle x | p_y | z \rangle = \sqrt{\tfrac{3}{2}} \langle \bar{x} | \bar{p}_x | y \rangle \tag{4}$$

is the momentum matrix element between the upper valence and second conduction band states.

If we make the reasonable assumptions that the spin-orbit splitting and k-linear terms of the second conduction bands can be neglected, and assume further that the dominant coupling of these bands is to the Λ_3 upper valence bands, then

$$E_c^0(k) = E_1 + \frac{\hbar^2 k^2}{2m_e}, \tag{5a}$$

$$E_v^0(k) = 0 + \frac{\hbar^2 k^2}{2m_e}\left(1 - \frac{4Q^2}{3m_e[E_1' - E_v(k)]}\right) . \tag{5b}$$

$$E_{SO}^0(k) = -\Delta_1 + \frac{\hbar^2 k^2}{2m_e}\left(1 - \frac{4Q^2}{3m_e[E_1' + \Delta_1 - E_{SO}(k)]}\right) , \tag{5c}$$

where E_1 and E_1' are the critical point energies of the E_1 and E_1' transitions, respectively, and Δ_1 is the spin-orbit splitting of the Λ_3 conduction bands. In Eqs. (5), we have taken the zero of energy to be at the top of the valence band.

These equations are most easily solved numerically. For computational purposes we take $E_1 = 3.46$ eV and $E_1' = 5.45$ eV, values that we determine experimentally. Because it is intrinsically impossible to measure Δ_1 directly in Si, we choose $\Delta_1 = 0.029$ eV $\cong \frac{2}{3}\Delta_0$, where $\Delta_0 = 0.044$ eV is the spin-orbit splitting of the upper valence bands at Γ.[27] We choose $Q = 1.00\hbar G_0$, roughly the average value along [111] as calculated by Cardona and Pollak.[18] Nominally $P = 2\pi\hbar/a_0$, but a more realistic estimate can be obtained if one fits P to the measured average transverse mass $\mu_T = 0.043\, m_e$ for Ge,[36] using Eqs. (1) and (5) with $\Pi_v = 0$ and appropriate energy gap data.[32] By so doing, we find $P = 1.32\hbar G_0$.

The intraband momentum matrix element Π_v varies from 0 at Γ through a positive maximum of about $0.15\hbar/a_B \cong 0.25\hbar G_0$ back to 0 at L.[25] Strictly speaking, this violates our assumption of cylindrical symmetry along each ⟨111⟩ direction. For simplicity, however, we shall retain approximately the cylindrical symmetry assumption by choosing $\Pi_v = 0.2\hbar G_0$, its average value over the middle third of a ⟨111⟩ symmetry axis. This value gives, using Eqs. (1) and (5), a transverse mass $\mu_{SO} = 0.022\, m_e$, the value reported by GH.[13] We justify this value of Π_v first as a reasonable weighted average, second in that it gives $\mu_{SO} = 0.022\, m_e$ for Ge, and third that these values of P, Q, and Π_v when used with the appropriate energy gaps[6] for the similar semiconductor GaAs yield $\mu_{SO} = 0.056\, m_e$, in excellent agreement with the measured value $0.055\, m_e$.[6]

The upper valence and lowest conduction band solutions of Eqs. (1) and (5) are shown in Fig. 1 for $\Pi_v = 0$ and for $\Pi_v = 0.2\hbar G_0$ for two values of ϕ. The conduction band is essentially unaffected by Π_v and ϕ, but the valence bands near $k = 0$ are strongly dependent on both Π_v and ϕ, as seen in Fig. 1. For nonzero Π_v, the valence bands are threefold periodic in ϕ, with extremum values occurring at $\phi = \pm\frac{1}{6}\pi + n\frac{2}{3}\pi$; $n = 0, 1, 2$. The energy bands in Fig. 1 are those corresponding to the extremum values of ϕ. The greatest change in the interband density of states occurs for $\phi = \frac{1}{6}\pi + n\frac{2}{3}\pi$, i.e., in a direction away from the nearest cube edge. For this value of ϕ and using the parameters given, the minimum energy separation be-

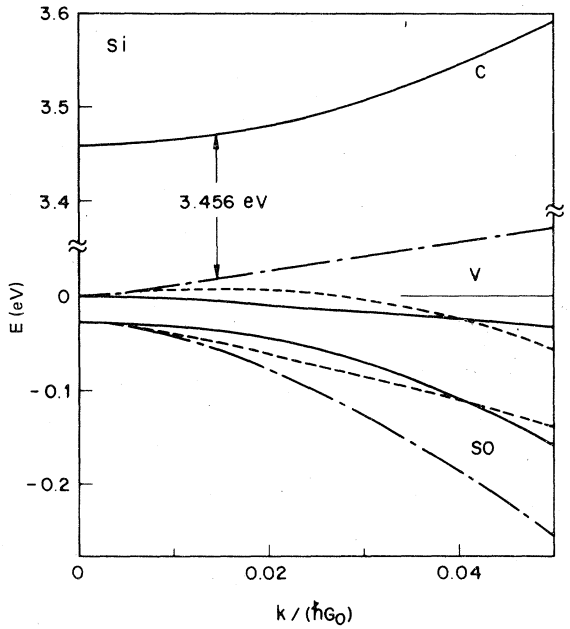

FIG. 1. $k_\perp$ dependence of the upper (v) and lower (SO) valence bands and of the conduction (c) band of Si along [111] in the five-band k-linear model, calculated for intravalence-band matrix elements $\Pi_v = 0$ (———), and $\Pi_v = 0.2\hbar G_0$ with $\phi = \frac{1}{6}\pi$ (-----) and $\phi = -\frac{1}{6}\pi$ (-·-). Other parameters are given in the text. The arrow locates the minimum energy separation of the v-c band pair for $\Pi_v = 0.2\hbar G_0$.

tween the v and c bands is 3.456 eV and occurs at $k = 0.0148\hbar G_0$, as shown in Fig. 1. At $k = 0$, the transverse interband mass is actually negative, $-0.10 m_e$. The nature of the off-axis critical

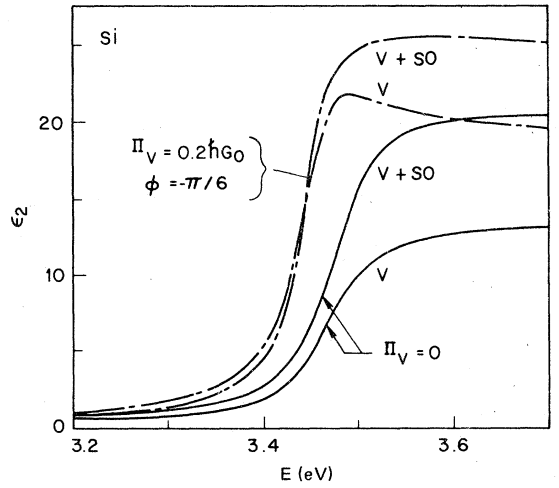

FIG. 2. Calculated values of ϵ_2 from the model band structure shown in Fig. 1, for $\Pi_v = 0$ and $\Pi_v = 0.2\hbar G_0$, $\phi = -\frac{1}{6}\pi$. Contributing bands are indicated.

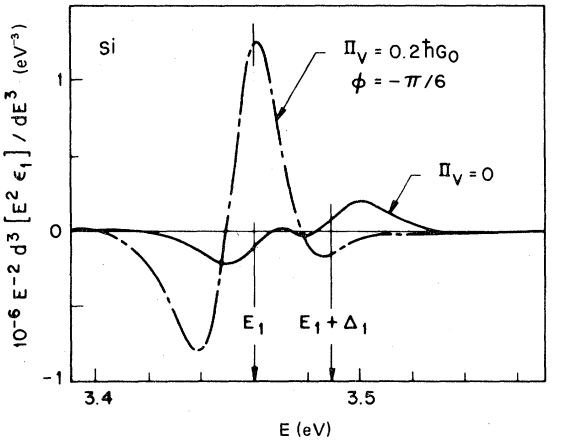

FIG. 3. Calculated third JDOS derivative of ϵ_1, for $\Pi_v = 0$ and $\Pi_v = 0.2\hbar G_0$, $\phi = -\frac{1}{6}\pi$.

points, either 3D M_0 or 3D M_1, is determined by the energy variation along [111].

For SO-c transitions, the critical point in all cases is at $k = 0$ and the dominant effect of Π_v is to lower the transverse interband mass at $k = 0$. For the parameters given, $\mu_T = 0.022 m_e$ as previously stated. The 3D M_0 or 3D M_1 character of this critical point is also determined by the energy variation in the [111] direction.

We next investigate the effects these nonparabolicities have on ϵ_2, the imaginary part of the complex dielectric function ϵ, on the third energy derivative of the joint density of states, and on the calculated low-field electroreflectance spectrum. Representative computations are shown in Figs. 2–4. The dielectric function ϵ_2 is evaluated according to the standard expression

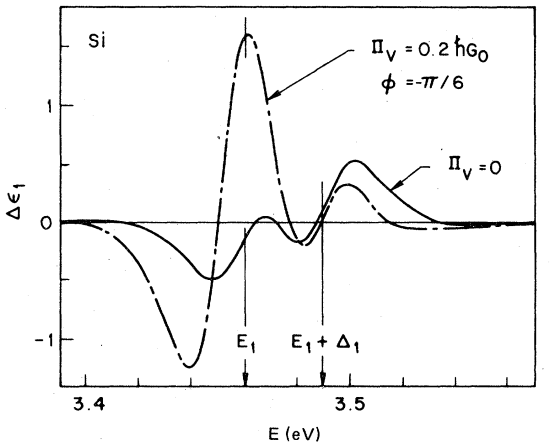

FIG. 4. Calculated low-field ER spectrum $\Delta\epsilon_1$ for $\Pi_v = 0$ and $\Pi_v = 0.2\hbar G_0$, $\phi = -\frac{1}{6}\pi$.

$$\epsilon_2 = \sum_{j=1}^{8} \frac{e^2(\hat{e}\cdot\vec{p}_{cv})^2}{\pi^2 m^2 \omega^2} 2\pi K_z \int_0^\infty \frac{k\,dk}{E_{cv}(k) - E - i\Gamma} \tag{6a}$$

$$= -\frac{1024\sqrt{3}\,(P/\hbar G_0)^2 \Omega^2(\mathcal{R}_\infty)}{15E^2(a_0/a_B)} \int \frac{z\,dz}{E_{cv}(z) - E - i\Gamma}, \tag{6b}$$

where we have substituted the value for K_z, evaluated for each direction the selection rule term involving the momentum matrix element and polarization vector, and used the definitions

$$\hbar\Omega = \hbar^2 G_0^2/(2\,m_e), \tag{6c}$$

$$(\mathcal{R}_\infty) = \hbar^2/(2\,m_e a_B^2) = e^2/(2a_B), \tag{6d}$$

where a_B is the Bohr radius. For clarity, we show only the contribution from the upper valence band and the total ϵ_2 curve for two sets of parameters: $\Pi_v = 0$, and $\Pi_v = 0.2\hbar G_0$, $\phi = -\pi/6$. This value of ϕ corresponds to that which maximizes the $E_1 + \Delta_1$ contribution and intersects an off-axis critical point. The rotational symmetry (ϕ independence) assumed in Eq. (6b) greatly simplifies the calculation without causing significant errors. These line shapes and also those in Figs. 3 and 4 were calculated using a broadening parameter $\Gamma = 0.030$ eV. This is the approximate value for[32] Ge and[6] GaAs at 10 K.

Figure 2 shows that the major effects of the k-linear term on the total ϵ_2 curve are to increase its value, particularly near threshold, and to shift it by about 30 meV to lower energy. Both effects result from the increased v-c interband state density near $k = 0$ with the broadening parameter acting to spread this increase to lower energy. The SO-c contribution is affected mainly by the reduction in magnitude that follows from the reduction in interband transverse mass with nonzero Π_v.

As shown in Fig. 3, the situation is quite different for the third joint-density-of-states (JDOS) derivative of ϵ_1, defined as $E^{-2}d^3(E^2\epsilon_1)/dE^3$. For $\Pi_v = 0$, the v and SO band contributions are nearly equal, because the dominant contribution comes from the Brillouin zone region immediately around $k = 0$ where the band curvatures are almost the same. But for $\Pi_v = 0.2\hbar G_0$, one observes a strong enhancement of the v-c structure and an almost complete suppression of the SO-c structure. Both $k = 0$ and $k = 0.0116 G_0$ thresholds appear higher in the main structure than expected from the three-point analysis[37] because of nonparabolicity effects.

Figure 4 shows a simulated $\Delta\epsilon_1$ spectrum calculated from low-field locally parabolic ER theory. For a simple parabolic, isotropic band pair c, v, low-field ER theory[2-4] shows that the ER spectrum is given simply by multiplying the third JDOS derivative spectrum by the prefactor

$$\tfrac{1}{3}(\hbar\Omega)^3 = e^2\mathcal{E}^2\hbar^2/24\,\mu_\parallel^{cv}. \tag{7}$$

where $\mu_\parallel^{cv}$ is the interband reduced mass in the direction of the electric field. By contrast, the exact one-electron expression[38] for nonparabolic, nondegenerate bands is complicated and requires multiple integrations. We have obtained the results shown in Fig. 4 by simplifying the exact theory to the case of locally parabolic bands. In this approximation the interband reduced mass in Eq. (4) is taken to be k dependent and is included as a factor in the integrand, which is evaluated at each point k according to the definition

$$[\mu_\parallel^{cv}(k)]^{-1} = (1/\hbar^2)[\hat{\epsilon}\cdot\nabla_{\vec{k}}]^2 E_{cv}(k), \tag{8}$$

where $\hat{\mathcal{E}}$ is the unit vector in the direction of $\vec{\mathcal{E}}$.

To evaluate Eqs. (7) and (8) for our specific case, it is necessary to consider each of the eight equivalent $\langle 111\rangle$ directions separately, calculate the angles that the field and polarization vectors make with each direction, evaluate the interband mass in the field direction, then weight each contribution according to its momentum matrix element. The general formulation is well known,[2,4] so we give only the results for the cases of interest: a [110] field with polarization vectors $\hat{e}$ parallel to $[1\bar{1}0]$ or [001]. For simple parabolic minima with finite transverse and longitudinal masses μ_t and μ_l, one finds

$$\frac{1}{\mu_\parallel^{cv}} = \begin{cases} \tfrac{1}{2}(1/\mu_l + 1/\mu_t), & \hat{e}_\parallel[1\bar{1}0] \quad (9a) \\ \tfrac{1}{3}(1/\mu_l + 2/\mu_t), & \hat{e}_\parallel[001]. \quad (9b) \end{cases}$$

For Fig. 4, we take $(1/\mu_l) = 0$ and $\mu_t = \mu_{cv}(\vec{k})$, as given by Eq. 4. To obtain explicit values, we have assumed that $E = 100$ kV cm^{-1}, and have divided spectra calculated with the mass of Eq. (5) by 2 to correct for $\mu_\parallel^{cv}$ as given by Eq. (9a).

The local parabolic band approximation reproduces qualitatively the effect of the acceleration mechanism, which enhances low-mass critical points relative to those with high mass. For Si with k-linear term included, this increases the contribution of the SO-c transitions relative to that of the v-c transitions, as seen by comparing Fig. 3 with Fig. 4. But Fig. 4 shows that this effect is not strong enough to influence significantly the density-of-states effect, and the overall line shape remains very similar to the third JDOS derivative shown in Fig. 3. The remnant of the SO-c structure appears as if it were only a subsidiary oscillation to the main structure, similar to experimental spectra.

With this background, we can comment on the

small mass measured in ER by GH, which was interpreted by Cardona[25] as arising from the SO-c transition near $k=0$. However, this requires that the SO-c contribution should dominate the ER line shape. Figure 4 shows rather that the v-c contribution dominates. But another possible explanation must be considered. If the k-linear effect is made arbitrarily large, then the mass of the resultant v-c critical line off $k=0$ can be made arbitrarily small. Thus in principle a small mass could be obtained even if the v-c transitions dominate; in this case the contribution from the region of negative mass near $k=0$ would be too small to be relevant. We must therefore estimate μ_t in the vicinity of the actual critical point of $k=0$ for $\Pi_v=0.2\hbar G_0$.

We do this by comparing peak-to-peak amplitudes of the third-derivative and $\Delta\epsilon_1$ ER structures and using Eq. (4) in the form [remembering that $\mu_{cv}=2\mu_t$ from Eq. (9a) for this calculation],

$$m_e/\mu_t = 48(\Delta\epsilon_1, ER)_{pp}/e^2E^2\hbar^2(J_3)_{pp}\,, \qquad (10)$$

where J_3 is the third joint-density-of-states derivative, and the subscript pp refers to peak-to-peak values.

For $\Pi_v=0$, this procedure leads to apparent transverse mass values of 0.061 m_e and 0.050 m_e for the v-c and SO-c structures, respectively. The average, $0.056\,m_e$, is somewhat larger than the $k=0$, $\Pi_v=0$ value 0.052 m_e for the v-c and SO-c pairs. This shows that nonparabolicity effects are already strong enough to invalidate simple arguments based on $k=0$ values for the mass even when the k-linear term is not included.

The same procedure for $\Pi_v=0.2\hbar G_0$, $\phi=-\frac{1}{6}\pi$ yields apparent transverse mass values of 0.107 m_e and $0.025m_e$, respectively, compared to calculated $k=0$ values of $-0.10m_e$ and $0.022m_e$. Thus both masses fall between their apparent values for $\Pi_v=0$ and their calculated $k=0$ values for $\Pi_v=0.2\hbar G_0$. The important point here is that the v-c apparent mass for $\Pi_v=0.2\hbar G_0$ is larger than its value for $\Pi_v=0$, so if the GH mass is to be recovered from the v-c structure, then Π_v must be substantially larger than current estimates.[25] This does not seem likely, whence we conclude that at this level of approximation, at least, theory does not support a small mass value for this transition.

We emphasize, however, that our ER calculation is quite crude, and that a more accurate model calculation would be necessary to give a thorough test. Such a calculation would be difficult because ideally one should include the Coulomb interaction,[33-35] a numerical evaluation of the general Franz-Keldysh integral,[38] and the variation of both Π (Ref. 24) and the interband energy[23,39] along the $\langle 111\rangle$ axes.

III. EXPERIMENTAL

The silicon samples used in these experiments were n-type single crystals having a resistivity of about 1 Ω cm at room temperature. The carrier concentration N_D was 5.7×10^{15} cm^{-3}. At this concentration field inhomogeneity effects are negligible.[4,40] Measurements were made or $\{110\}$ surfaces because these give the maximum symmetry information in surface-barrier ER measurements.

Samples were prepared by sandblasting and rhodium plating the back surface to form the ohmic contact, then evaporating a semitransparent Ni layer 3–4 nm thick on the Syton-polished front surface to form the Schottky barrier. Details have been given elsewhere.[7] ER spectra were measured using standard phase-sensitive detection techniques.[1]

Dielectric function spectra were obtained using the high-precision rotating-analyzer ellipsometer described previously.[28] All data were obtained on naturally oxidized Si surfaces. These data were corrected analytically for the presence of the approximately 25-Å natural oxide layer[41] and for the optical activity of the quartz Rochon prisms.[42] Room-temperature measurements were performed with the sample in air. Low-temperature measurements were performed with the sample mounted on the cold finger of the liquid-He transfer-line cryostat.[43] Because the room-temperature cryostat pressure was of the order of 10^{-6} Torr, the sample adsorbed gas at the rate of approximately $\frac{1}{2}$ Å/min at 10 K. Thus ellipsometry data were taken as rapidly as possible at low temperature. Where necessary, the low-temperature data were also corrected for the effects of the adsorbed gases, although this correction was of minor importance when these data were differentiated numerically to obtain calculated higher-derivative spectra.

Electric field values were determined from the measured doping of the crystal as determined from Schottky barrier capacitance values.

IV. RESULTS AND DISCUSSION

An overview of the complete ER spectrum up to 6 eV is shown in Fig. 5. This spectrum was taken at a sample temperature of 10 K and at a relatively high value of the modulating field. Structure is labeled according to the standard convention. Previous work[8-23] has established the identity of the transitions giving rise to these structures as follows: E_0': upper valence to Γ_{15} (lowest) conduction band; E_1: upper valence to lower conduction bands along the $\langle 111\rangle$ directions; E_0: upper valence to $\Gamma_{2'}$ conduction band; E_2 doublet: not clear but probably involving the $\langle 110\rangle$ directions;

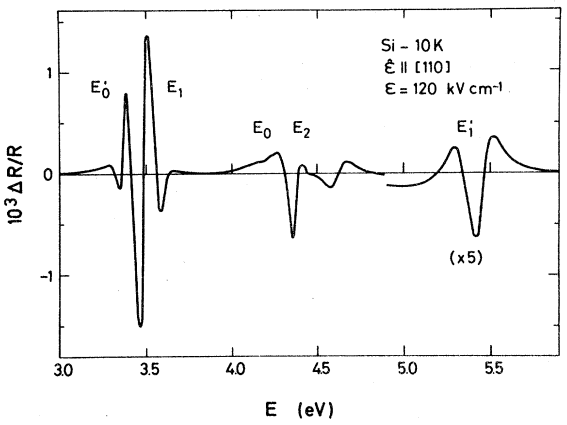

FIG. 5. Complete ER spectrum of Si to 6 eV at 10 K, taken with a relatively large value of the electric field.

E_1': upper valence to second conduction bands along the ⟨111⟩ directions. The E_0' and E_1 transitions are overlapping but resolved. The E_1' transition is weak and was investigated only with unpolarized light.

Dielectric function data from 3.0 to 5.5 eV are shown in Figs. 6 and 7. These figures give the real (ϵ_1) and imaginary (ϵ_2) parts, respectively, of the complex dielectric function ϵ, measured at 293 and 10 K and corrected as indicated in Sec. III. The insets in these figures illustrate structural details near the E_0' and E_1 thresholds in these data, to be discussed in the following section.

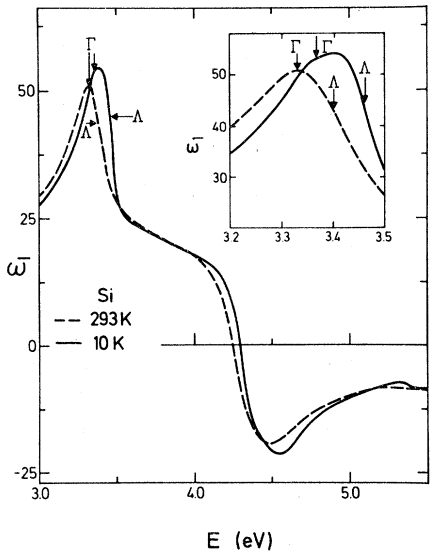

FIG. 6. Real part ϵ_1 of the complex dielectric function of Si from 3.0 to 5.5 eV, measured ellipsometrically at 293 and 10 K.

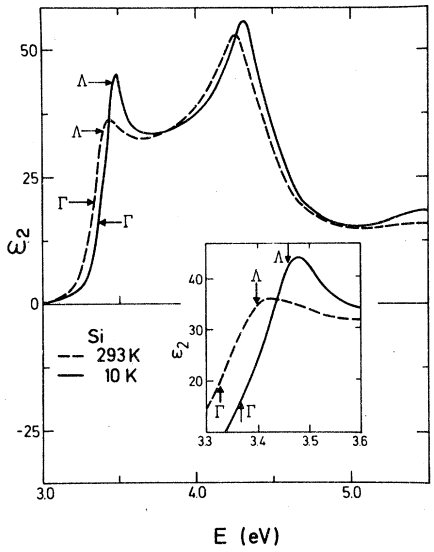

FIG. 7. Imaginary part ϵ_2 of the complex dielectric function of Si from 3.0 to 5.5 eV, measured ellipsometrically at 293 and 10 K.

A. E_0' and E_1 transitions

Before analyzing these data in detail, we note that a comparison of Fig. 7 with Fig. 2 shows that one-electron theory is only approximately valid. The actual E_1 threshold in Fig. 7 occurs at an ϵ_2 value near 36, about 33% larger than the calculated value shown in Fig. 2. A shift of oscillator strength to lower energies as a result of the Coulomb interaction is well known.[44] The strongly peaked threshold in the 10-K ϵ_2 data also shows that a significant electron-hole enhancement is present.

Our ER data agree in line shape and magnitude with those previously reported by KM and GH when taken under similar conditions of temperature and surface field. Because we investigate both room-temperature and low-temperature line shapes to lower field values than those previously reported, and because we compare these ER spectra to numerically differentiated ellipsometric data, our results show some basic differences that lead in some cases to different interpretations of the energy band structure giving rise to these transitions.

1. Number of critical points

Figure 8 shows room-temperature ER spectra taken over a range of field values down to 42 kV cm^{-1}. In addition to the well-established E_0' and E_1 structures near 3.32 and 3.4 eV, respectively, the lowest-field spectra show additional structure near 3.5 eV.

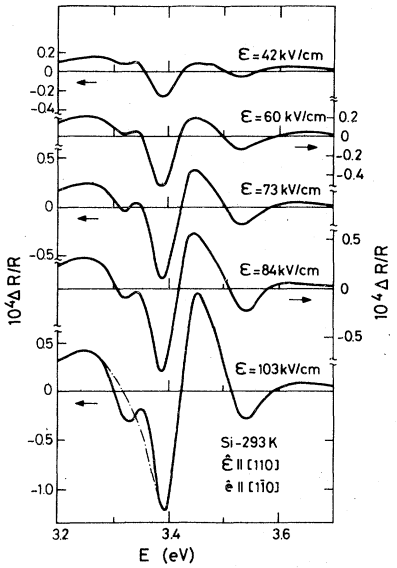

FIG. 8. Evolution of the 293-K $\Delta R/R$ line shape of the E_0' and E_1 structures with increasing field.

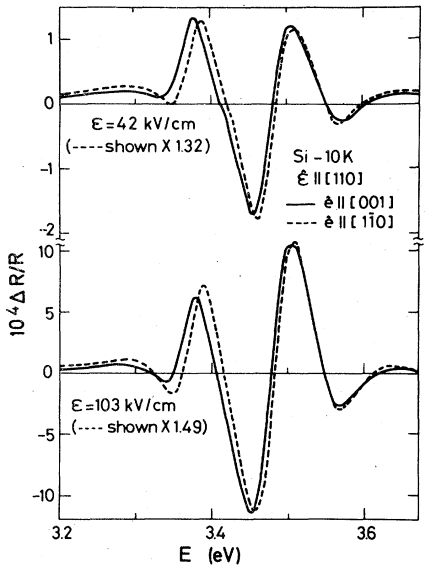

FIG. 10. As Fig. 9, but at 10 K.

In order to investigate the extra structure further, polarization measurements were performed. These give clear evidence at room temperature of the existence of the third critical point, as shown in Fig. 9. Here, spectra are shown for low and moderate field values for the two principal polarizations. The spectra for $\hat{e}\parallel [1\bar{1}0]$ are multiplied by factors of 1.41 and 1.54 for 42 kV cm^{-1} and 103 kV cm^{-1}, respectively, in order to bring the principal positive and negative peaks into coincidence with the $\hat{e}\parallel$ [001] results and thus facilitate line-shape comparison. The E_0' structure at 3.32 eV shows an opposite anisotropy.

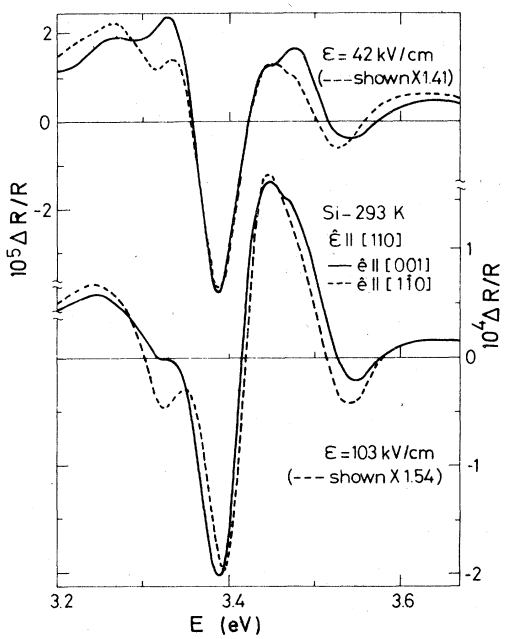

FIG. 9. Polarization dependence of the lower-energy structures in ER measured at room temperature.

The third critical point, probably near 3.50 eV, has an anisotropy opposite that of E_1. It therefore cannot be related to the spin-orbit-split valence band but must originate in other regions of the Brillouin zone. It gives rise to a well-defined structure at very low fields but only a relatively weak shoulder at moderate fields. It was overlooked by GH apparently for this reason.

By contrast to the room-temperature data, at 10 K, only the E_0' and E_1 structures can be observed. In Fig. 10, the anisotropy factors are 1.32 for 42 kV cm^{-1} and 1.49 for 103 kV cm^{-1}. The polarization anisotropy of the E_0' structure is more nearly like E_1, by contrast to the room-temperature case.

The absence of apparent structure from the third critical point in the low-temperature spectra is easily explained if it arises from non-Λ transitions, as the room temperature polarization data show. Figures 9 and 10 show that the E_0' and E_1 structures shift 40 and 70 meV, respectively, to higher energy upon cooling from 293 to 10 K. This is consistent with the corresponding shifts in other materials[45] and simply reflects the relatively large admixture of volume-sensitive s-wave functions into the Λ states. If the third transition has a temperature shift of mainly p-state origin, such as the E_0' structures, then Fig. 9 shows that it

would be buried under the E_1 structure at low temperature. It appears to have been overlooked by KM for this reason.

Unfortunately, it was not possible to confirm the existence of the third critical point by ellipsometry, nor was it possible to obtain detailed information about its line shape, owing to overlap with the E_1 structure. Nevertheless it is clear that its presence will exert some influence on polarization ratios, line-shape analyses, and stress measurements of the nominally E_1 structure, particularly at low temperature, where the two cannot be separated.

In Fig. 10, the shifts of 10 and 6 meV between the polarization spectra for the E_0' and E_1 transitions, respectively, are real.

2. *Band nonparabolicity*

The spectra of Fig. 8 show another unusual feature: the E_1 line shape continues to change with decreasing field down to our practical limit of 42 kV cm^{-1} at room temperature, at which point the maximum amplitude of $\Delta R/R$ is only parts in 10^5. The change is most prominent in the asymmetry of the E_1 structure, where the positive peak grows rapidly relative to the rest of the line shape. No energy shifts are seen. Inhomogeneity is not the cause since the E_2 structure with a similar large value of ϵ_2 shows a well-defined low-field line shape.

The effect appears to be unique to Si. Similarly doped crystals of Ge,[4,32] GaAs,[6] and[46] GaSb show well-defined low-field regions for E_1 and $E_1+\Delta_1$.

Theory predicts that the low-field limit is reached when

$$\tfrac{1}{3}\Gamma = \hbar\Omega_{\mathrm{LF}}, \tag{11}$$

where $\hbar\Omega$ and μ_{cv} are given by Eqs. (7) and (9) with $\mu_l^{-1}=0$. Figure 4 shows that the primary contribution to the ER spectrum comes from the v-c transitions, which have a calculated apparent mass ranging from $0.061m_e$ for $\Pi_v=0$ to $0.107m_e$ for $\Pi_v=0.2\hbar G_0$. If $\Gamma\cong 52$ meV, the GH result, then the masses would indicate a value of $\mathcal{E}_{\mathrm{LF}}$ near 80–110 kV cm^{-1}. But Fig. 8 shows that the line shape is still changing rapidly at this field value. Thus the result is surprising from theoretical grounds as well as from previous measurements on related semiconductors.

The lack of a low-field limit is probably not unreasonable when one considers that the acceleration of an electron by the electric field causes it to sample a range of momentum space during its lifetime and thus act as if it had an apparent mass depending on the nonparabolicity, field, and broadening. This effect is not included in the locally parabolic model line shapes discussed in Sec. II. It was previously used to explain the anomalous field dependence of the 4.6-eV E_0' complex on GaAs.[6]

Quantitatively, the relative range in k space is

$$\Delta k/G_0 = e\mathcal{E}a_0/2\pi\Gamma, \tag{12}$$

where we have used the approximation $\tau\approx\hbar/\Gamma$ for the electron lifetime. At $\mathcal{E}=42$ kV cm^{-1}, $\Delta k/G_0$ ~ 0.007, which is comparable to the k-space separation between the critical line and $k=0$. Moreover, Fig. 1 was calculated with $\Pi=0.2\hbar G_0$, whereas, in fact, Π_v varies from 0 at each end of the Λ axis to some maximum near the middle. Thus there are always regions of the $\langle 111\rangle$ axes where nonparabolicity effects are significant for any range of Δk.

The role of intravalence band coupling is therefore to insure the presence of locally nonparabolic regions somewhere along the $\langle 111\rangle$ directions. Whether these nonparabolicity ranges contribute sufficiently to explain the effect should be tested by more accurate calculations. GaP should also show a similar absence of a low-field spectrum for the E_1 structure, owing to its small value of spin orbit splitting; however, GaP has not been investigated by low-field Schottky-barrier ER.

3. *Polarization anisotropies in ER spectra*

From Fig. 9, polarization ratios of 1.41–1.54 were obtained at room temperature for the E_1 structure. The average scaling factor for the available field range was 1.52. At 10 K, an average value of 1.43 was obtained. These values are about 15% larger than those found for the E_1 transitions in[32] Ge and GaAs,[6] which were 1.32 at room temperature and 1.20 and 1.22, respectively, near 10 K. They are also larger than the KM low-temperature value of 1.35, which was based on the anisotropy of the positive E_1 peak alone. The KM value would actually be reduced further to 1.27 if calculated on a peak-to-peak basis, as we have done here.

Low-field theory predicts that the polarization anisotropy depends only on the longitudinal and transverse mass ratios for simple parabolic bands. Specifically, for $\vec{\mathcal{E}}_{\parallel}[110]$ and $\hat{e}\|[1\bar{1}0]$ or $\hat{e}\|[001]$, low-field theory shows that

$$\frac{(\Delta R/R)_{[001]}}{(\Delta R/R)_{[1\bar{1}0]}} = \frac{4}{3}\,\frac{1+\mu_t/2\mu_l}{1+\mu_t/\mu_l}. \tag{13}$$

For Ge and GaAs at room temperature (probably a more representative case since exciton effects are more important at low temperature), Eq. (13) predicts $|\mu_l|\gg\mu_t$, in essential agreement with recent band structure calculations.[22,23]

A ratio 1.43 is obtained if $\mu_l \cong -8\mu_t$. The negative value indicates an M_1 singularity, in agreement with the KM conclusions, although their data are in fact marginal on this point. The actual longitudinal mass value based on this ratio is surprisingly small: taking for μ_t the $\vec{k}\cdot\vec{p}$ value of 0.052 m_e, the energy should decrease by over 1 eV at the zone boundary if the simple parabolic M_1 critical point is located in the middle of the $\langle 111\rangle$ axis. Such a large curvature is not likely.

However, another possibility exists. If the apparent transverse mass is much larger, then μ_l could also be much larger, while maintaining the ratio of 8 and yielding a reasonable curvature. We view this as a more likely possibility.

Theory including k-linear coupling predicts that the transverse mass for the v band should be larger than that of the SO band. Direct evidence for this comes from the noticeable shift of the E_1 line shape to lower energy for [001] polarization, which is seen most clearly in the 10-K data. We interpret the effect as follows. We note first that the longitudinal masses for both v and SO bands should be the same because the spin-orbit splitting is constant over most of the $\langle 111\rangle$ axis. If now the transverse mass were larger for v than for SO, then the anisotropy would be larger for v-c than for SO-c, by Eq. (13). Thus the [001] spectrum contains a larger contribution from the v band than does the $[1\bar{1}0]$ spectrum. If the spin-orbit splitting is too small to be resolved, then the larger v contribution will cause the [001] line shape to appear to shift to lower energy, as observed in Fig. 10. We therefore interpret this shift as evidence for the larger transverse mass of the v band caused by the intravalence band coupling. Again, because of its small spin-orbit splitting, a similar effect should be observed in GaP.

Because the dominant E_1 structure arises from an M_1 critical point, substantial oscillator strength below its energy could be expected. This oscillator strength does in fact appear in the ellipsometric spectra and will be discussed in Sec. IV A5.

The anisotropy ratio of the E_0' structure was determined to be 1.17 from 10-K data shown in Fig. 10. This is in very good agreement with the value 1.15 obtained for Ge.[32]

4. *ER line-shape analysis and critical-point energies*

While polarization anisotropy and field dependences may be studied with $\Delta R/R$ spectra, line shape analysis must be performed on $\Delta\epsilon$ spectra. The rapid change in ϵ with wavelength in the 3.4-eV range invalidates the assumptions necessary to apply the three-point method.

Figure 11 illustrates the difference between a

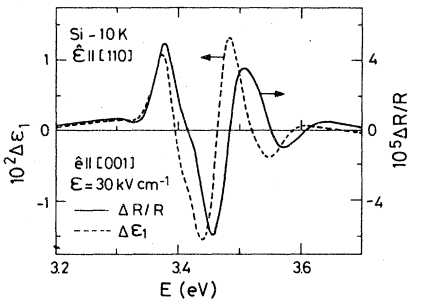

FIG. 11. Comparison of $\Delta R/R$ line shape with $\Delta\epsilon_1$ calculated from it using the optical data of Figs. 6 and 7.

$\Delta R/R$ spectrum and the real part of its Kramers-Kronig transform, calculated by means of the dielectric function data of Figs. 6 and 7. The spectra agree below 3.37 eV where ϵ_2 is small, but differ at higher energies, particularly with respect to peak positions. $\Delta\epsilon_1$ data at a higher field value are shown in Figs. 12 and 13 for 293 and 10 K, respectively.

Detailed analysis is very difficult because of overlapping structures. But in agreement with previous work, we assign the main negative and positive peaks to the E_1 structure, for the following additional reasons. The temperature shift of these peaks is large, consistent with E_1 transitions in other materials, and if the shallow positive tail below 3.3 eV is included (see Fig. 12) the line shape is very similar to the E_1 line shapes in Ge and GaAs.

By including the low-energy tail in the E_1 line

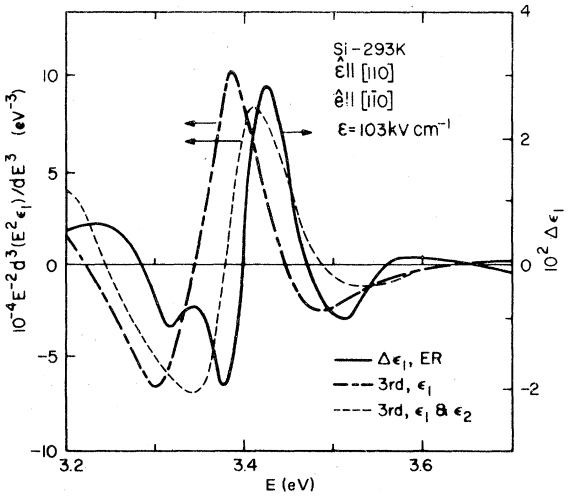

FIG. 12. Comparison of $\Delta\epsilon_1$ and third JDOS derivative line shapes at 293 K.

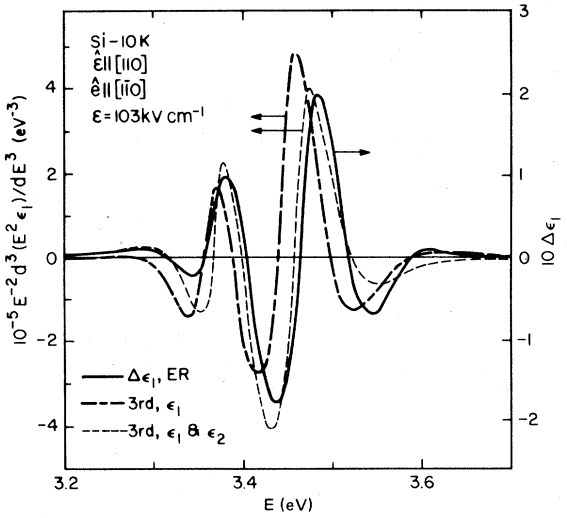

FIG. 13. As Fig. 12, but for 10 K.

shape, we can interpret the E_0' structure as a M_0 critical point superimposed on the E_1 tail. The E_0' structure than has an M_0 character at room temperature, as well as at 10 K. This resolves the M_1 interpretation of GH, made on the basis of theoretical simple parabolic low-field line shapes fit to data. Because the simple line shapes cannot represent the E_1 low-energy tail, a theoretical fit over the entire spectrum should not be expected, nor forced.

The assignment of the E_0' structure to Γ_{15} transitions is well accepted. We find in agreement a polarization anisotropy and temperature shift similar to those observed in Ge for these transitions.[32]

At 10 K the E_0' and E_1 structures are better separated owing to overall sharpening and different temperature coefficients, although the E_0' structure is clearly seen even at room temperature. Using these $\Delta\epsilon_1$ data, we find threshold energies as given in Table I. These are also compared to other data and to band-structure calculations.

5. *Ellipsometric data*

ϵ_1 and ϵ_2 are shown at 10 and 293 K in Figs. 6 and 7. The energies of the Γ and Λ critical points determined in the preceding section are indicated.

The general shape of the ϵ_1 spectrum is not much changed by cooling. However, a close examination of the 3.4-eV peak for the 10-K spectrum (see inset) shows that a shoulder has developed 50 meV below the main peak. Ths shoulder is not seen in the room-temperature spectrum. The main peak shifts 70 meV upon cooling.

The ϵ_2 spectra show more changes. The 3.4-eV peak becomes sharply enhanced and much narrower at 10 K, suggesting exciton effects. The peak itself moves 55 meV to higher energy at 10 K. A close examination for fine structure shows only a break about 80 meV below the main peak in the 10-K curve, and nothing in the 293-K data.

It is remarkable in the ϵ_2 curve that much of the oscillator strength lies below the energy of the Λ singularity itself. This is consistent with an M_1 interpretation of this critical point, as it suggests a distribution of oscillator strength along the $\langle 111\rangle$ axes down to the $E_0'M_0$ threshold at Γ. The overall shape at room temperature is similar to that of Ge, where the bands remain nearly parallel for much of the $\langle 111\rangle$ axes,[47] and where most of the 1.3 eV decrease between the M_1 singularity at L and the M_0 direct gap at Γ occurs in the 20% nearest Γ.[48] As in Ge, the ER data provide no direct evidence for M_0 critical points at L although they cannot be ruled out if they are weak and/or overlap the E_0' structure. We view the latter possibility as unlikely.

6. *Comparison of ER and ellipsometric spectra*

Direct comparisons between $\Delta\epsilon_1$ and the third JDOS derivative are shown in Figs. 12 and 13 for 293 and 10 K, respectively. The greater broadening at room temperature decreased the third derivative amplitude sufficiently so that the E_0' structure could not be resolved, even if it were present to the extent that it appears in the ER spectrum. Also at room temperature, an energy shift is seen that gets increasingly larger at lower energies. From 20 meV at the highest-energy negative peak, this separation increases to 30 meV at the positive peak, 50 meV at the zero crossing, and 80 meV at the lowest-energy negative peak. The fact that the shift increases also with the width of the structures suggests that it may be due to only a phase shift of the type previously observed for Ge,[3] where an equal admixture (45° phase shift) of third-derivative line shapes was found to give the best agreement with experiment. Previous comparisons for these structures at room temperature also pointed to a phase shift of about 60°.[30]

Accordingly, we show also the calculated spectrum with ϵ_1 and ϵ_2 weighted by 1.0 and 1.5, respectively, and normalized to $\sqrt{3.25}$. As seen, agreement is improved, although not completely restored. Calculations for $\Pi_v \cong 0.2\hbar G_0$ in the locally parabolic model show similar behavior between third-derivative and ER spectra, although such shifts are smaller, only of the order of several meV. We interpret the shift as being due partly to this effect, partly to the $[1\bar{1}0]$ polarization ef-

fect discussed previously, and partly to the sensitivity of the ellipsometric data to noncritical point regions along [111] that ER does not pick up. The phase shift itself was attributed previously to an increase in broadening parameter with increasing energy,[3] owing to the decrease in expected lifetimes resulting from the increasing number of final states into which the electrons and holes can scatter.

At 10 K, the line shapes are in much better agreement and the energy shift is much less, about 25 meV for E_1 and 10 meV for E_0'. If the phase is allowed to vary, i.e., if linear combinations of the real and imaginary parts are again formed to obtain a better fit, then the shifts can be nearly eliminated and also the line shape asymmetries brought into better agreement, as seen in Fig. 13. Thus the third-derivative relation predicted by the low-field theory appears to be qualitatively valid for these structures as well.

Using the analysis in Sec. II, we calculate apparent transverse masses of $0.58m_e$ at room temperature and $0.33m_e$ at 10 K. These are significantly larger than the values $0.06m_e$–$0.11m_e$ calculated for $0<\Pi_v<0.2\hbar G_0$, and indicate that the ER spectrum is too small relative to the third derivative. By comparing Figs. 2, 3, and 4 with Figs. 7 and 13, respectively, one finds that at 10 K the measured ϵ_2 spectrum is about 1.4 times larger than expected, the third derivative spectrum is about 2.6 times smaller than expected, and the ER spectrum is about 7 times smaller. While the absolute values of the ER and third-derivative spectra depend upon the choices of Π and Γ, the relative values do not. The fact that the ER to third-derivative ratio is too small gives direct evidence for the Coulomb interaction. We note that the more rapid growth of the ER spectrum with decreasing temperature is a further indication of this because ER is more sensitive to the critical point, while ellipsometry obtains contributions from noncritical regions as well. The smaller ER spectrum is significant because its amplitude is independent of the transverse mass in the 2D limit, in which case a discrepancy can come only from electron-hole final-state interactions.

The average increase of factors of 4.4 and 7.8 in the third-derivative and ER data, respectively, from 293 to 10 K imply a decrease of broadening of factors of 1.64 and 1.98, respectively, in the simple model neglecting Coulomb effects. Taking a mean value and using the GH result of 52 meV at room temperature indicates that the broadening at 10 K is about 29 meV, in agreement with that of Ge and GaAs. Because it is of the same order as Δ_{SO}, and because of the intravalence band coupling, no spin-orbit-split structure can be resolved, in agreement with experiment.

B. E_0 and E_2 transitions

The spectral region from 3.9 to 4.9 eV shows three distinct structures, the E_0 transition near 4.2 eV and two E_2 structures near 4.4 and 4.6 eV. Representative ER spectra, transformed to $\Delta\epsilon_1$, are shown at 293 and 10 K in Figs. 14 and 15, respectively. These transitions are less field and temperature dependent than those in the E_0', E_1 region of the spectrum, and consequently less information can be deduced about them. We discuss primarily the polarization anisotropies, and comment about the ER and ellipsometric line-shape comparisons.

1. Polarization anisotropy

Only a small anisotropy was observed for the E_0 and $E_0+\Delta_0$ transitions. These transitions are weak and can be resolved clearly only below 80 K. Because they also overlap the E_2 structure, the asymmetry was not possible to analyze. Essentially no anisotropy is expected because of the final-state symmetry of these transitions.

The asymmetry ratio of the main E_2 structure near 4.3 eV is somewhat field and temperature dependent, as seen in Figs. 14 and 15. At room temperature, the $\hat{e} \parallel [1\bar{1}0]$ spectra must be multiplied by factors of 1.61 and 1.72 for $\mathcal{E}$ equal to 42 and 103 kV cm^{-1}, respectively, to bring the positive peaks into coincidence. The lower and higher parts of the 4.3-eV structure show less anisotropy.

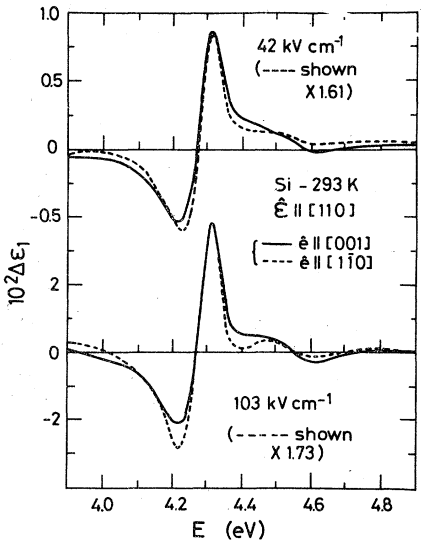

FIG. 14. $\Delta\epsilon_1$ spectra at 293 K for the E_2 transitions.

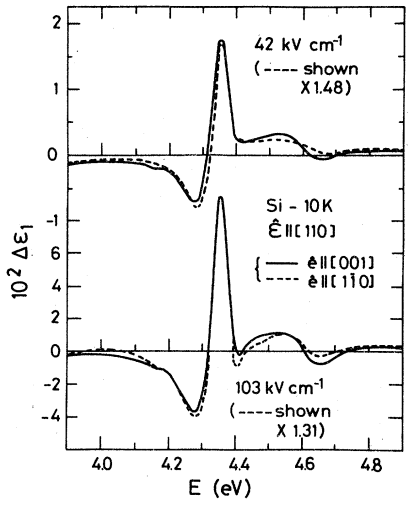

FIG. 15. As Fig. 14, but for 10 K.

By contrast, the 4.6-eV structure shows a larger anisotropy of about 2.5. No shift of the line shape with polarization can be detected.

At 10 K all anisotropy ratios decrease, in agreement with the observations on the E_0' and E_1 structure. Here, the anisotropies of the 4.3-eV structure are 1.48 and 1.31 for 42 and 103 kV cm^{-1}, respectively. The anisotropy of the peak is less at higher fields, by contrast to the room temperature measurement. The anisotropy is also less for the lower and higher parts of this structure. For the 4.6-eV structure the anisotropy is also less, 2.1. Except for the negative peak at 4.26 eV, no energy shift can be detected.

The large difference in anisotropy shows that the E_2 structures at 4.3 and 4.6 eV arise from different critical points and possibly even from different regions of the Brillouin zone. While the different line shapes also suggest this, definite proof comes from the alloy measurements of Kline *et al.*,[49] which show that the 4.6-eV structure vanishes when Si is diluted by about 9% Ge. Thus the lower E_2 structure appears to be related to the E_2 structures in Ge, which also follows from the similarity in their anisotropy ratios even though the line shapes are somewhat different. It may not be true for GaAs, for which the anisotropy ratio of the corresponding transition is much less.

The large anisotropy shows that at least one negative mass is involved for these critical points. We have not observed Franz-Keldysh oscillations above E_2, however, as seen for Ge.[32,37] Nor do we observe a significant change of the line shapes with field, suggesting that even at the highest fields we are in the low-field limit. Surprisingly, this E_2 line shape resembles fairly closely the E_1 line shape, with a sharp positive peak and a relatively long low-energy tail. We do not find it necessary to postulate a third critical point near 4.5 eV as done by KM.[16]

2. *Ellipsometric data*

The variations of ϵ at 10 and 293 K in the E_2 region are shown in Figs. 6 and 7. Not as much change is observed here as for the E_1 structure although the structures do sharpen and the peaks move to higher energy with cooling. At 10 K, Fig. 6 shows the existence of a weak break that corresponds to the onset of the second E_2 transition in the ER data.

3. *Comparison of ER and ellipsometric data*

By contrast to the previously discussed situation there is no obvious connection between $\Delta\epsilon_1$ and the third JDOS derivative in the E_2 region, as indicated in Fig. 16. One could achieve better agreement by superimposing real and imaginary parts of the third JDOS derivative. But the best agreement, particularly for the 4.3-eV structure, comes from the second derivative, which is also shown in Fig. 16. The modified third derivative has the same line shape but the peaks are somewhat too narrow. The large phase angle of 110° necessary to achieve qualitative line-shape agreement with the third derivative seems difficult to justify.

The second-derivative connection is also puzzling. Effectively, a second-derivative-like line shape could be obtained three ways. First, the field could be influencing the broadening parame-

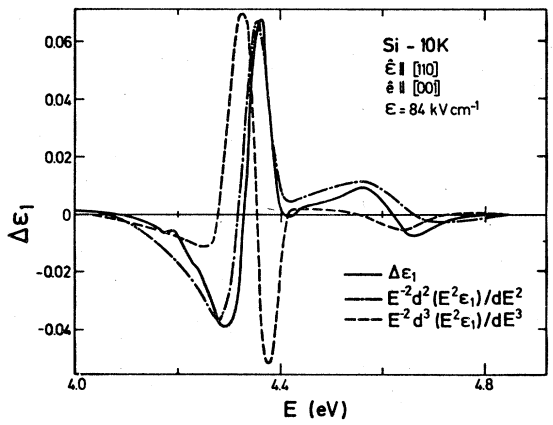

FIG. 16. Comparison of $\Delta\epsilon_1$ and third JDOS derivative line shapes for Si in the E_2 spectral region at 10 K. The peak-to-peak values of the second and third JDOS derivatives are 5.5×10^3 eV^{-2} and 2.2×10^5 eV^{-3}, respectively.

ter directly. This is most unlikely. Secondly, the field could induce a third derivative with respect to the broadening parameter. This is unphysical. Thirdly, the regular third-derivative mechanism could be shifted by 110°. This is most probable but the calculated line shapes are somewhat narrower than the observed $\Delta\epsilon_1$ ER spectra. We note that Blossey's theory[34] cannot be differentiated to obtain a second-derivative line shape either.

Supposing that the third-derivative connection remains valid, we can still determine the apparent interband mass by means of Eq. (6). Because a μ_l, μ_t separation is meaningless we give simply μ_{cv}. Taking the [001] polarization spectra as having the largest size and therefore the smallest mass we find values of about $0.25m_e$ and $0.22m_e$ at 10 and 293 K, respectively. The estimate for the 4.6-eV structure is somewhat less, $0.12m_e$. The first value is somewhat larger than that, $0.14m_e$, obtained for the corresponding transition in Ge from analysis of Franz-Keldysh oscillation,[32,37] which is consistent with the behavior observed for the E_1 transition in Si.

C. Band structure

The present work confirms the multiplicity of critical points in the 3.4-eV region which was observed previously by various authors. From the preceding two sections, we can say that the E_1 region is characterized by an M_0 transition at 3.365-eV (all 10-K values) and an M_1 transition at 3.46 eV. These are the E_0' and E_1 transitions, respectively. The most likely position for the E_1 critical point is at L, with the energy decreasing monotonically along $\langle 111\rangle$ from L to Γ. A third critical point near 3.5 eV, not along $\langle 111\rangle$, has been deduced from room-temperature data, but it cannot be separated from the stronger E_1 transition at 10 K. The strongest evidence for k-linear valence-band coupling comes from the line shape of the E_1 structure, which appears very similar to that calculated in the locally parabolic low-field limit in that only the upper valence band contributes and the spin-orbit-split valence band is strongly suppressed. Contrary to initial interpretation,[25] it is the SO-c transitions that cannot be seen in ER spectra.

The E_0, two E_2, and E_1' structures have been Kramers-Kronig transformed and their threshold energies determined by the three-point method at various temperatures. These data are summarized in Table I and compared to other experimental work. Most numbers are in general agreement, although we differ substantially from the 293-K E_0' critical-point energy determined by GH.[13] This is a result of their M_1 interpretation and not due to any essential difference in data. We differ from KM for E_2 in that we do not find it necessary to invoke a third critical point in the E_2 structure.

The detailed investigation of the ER spectrum and the resolution achieved allow a close comparison with the most accurate band-structure calculations. The results of several such are also shown in Table I. Before the positive identification of the E_0 threshold in Si,[12] these calculations tended to place the threshold anywhere within a general range of 3–4.5 eV. Recent calculations by Saravia and Brust[21,22] and Chelikowsky and Cohen,[23] which provide probably the most accurate computations to date, place the E_0 threshold correctly and calculate the remaining band structure from adjustable pseudopotential coefficients.

From Table I, we conclude that the Chelikowsky-Cohen calculation is slightly better in that it places the E_0' and E_1 thresholds most accurately. The Saravia calculation provides information about other critical points in the 3.4-eV region, but our data are too poor on the third structure to suggest an assignment. The nearly two-dimensional nature of the energy bands in Si, as interpreted by GH,[13,47] is also supported by our results.

The anomalously small mass observed by GH was derived from a fitted value of $\hbar\Omega$. We find no evidence for a small mass, although we did not reach fields as high as GH. We believe that GH obtained a larger-than-real value of $\hbar\Omega$ because they used a model which was inadequate to represent the complicated band structure in the E_1 region. The theoretical calculations of the effect of the k-linear term do not support a low mass value either, but show instead that the k-linear effect acts mainly to transfer oscillator strength from the SO-c transitions to the v-c transitions and to increase the apparent mass of this transition. It is unlikely that a more accurate calculation would lead to a qualitatively different conclusion.

ACKNOWLEDGMENTS

The authors gratefully acknowledge the technical assistance of A. A. Studna. One of us (A.D.) is grateful to Bell Laboratories for their hospitality during this work, and wishes to thank the financial support of a NATO Fellowship. One of us (D.E.A.) wishes to thank the Alexander von Humbolt Foundation and the Max-Planck-Institut für Festkörperforschung, Stuttgart, where part of this work was done, for their support and hospitality. We also wish to thank M. Cardona for an unpublished report of his results prior to publication.

*Laboratoire Associé au CNRS No. 232.
[1](a) M. Cardona, *Modulation Spectroscopy* (Academic, New York, 1969); (b) B. O. Seraphin, in *Optical Properties of Solids*, edited by F. Abeles (North-Holland, Amsterdam, 1972), p. 163; (c) *Semiconductors and Semimetals*, edited by R. K. Willardson and A. C. Beer (Academic, New York, 1972), Vol. 9; (d) Y. Hamakawa and T. Nishino, in *Optical Properties of Solids: New Developments*, edited by B. O. Seraphin (North-Holland, Amsterdam, 1976), p. 255.
[2]D. E. Aspnes and J. E. Rowe, Solid State Commun. 8, 1145 (1970); Phys. Rev. B 5, 4022 (1972).
[3]D. E. Aspnes, Phys. Rev. Lett. 28, 168 (1972).
[4]D. E Aspnes, Surf. Sci. 37, 418 (1973).
[5]D. E. Aspnes, Phys. Rev. Lett. 28, 913 (1972).
[6]D. E. Aspnes and A. A. Studna, Phys. Rev. B 7, 4605 (1973).
[7]A. A. Studna, Rev. Sci. Instrum. 46, 735 (1975).
[8]R. R. L. Zucca and Y. R. Shen, Phys. Rev. B 1, 2668 (1970); R. R. L. Zucca, J. P. Walter, Y. R. Shen, and M. L. Cohen, Solid State Commun. 8, 627 (1970).
[9]R. Braunstein and M. Welkowsky, in *Proceedings of the Tenth International Conference on the Physics of Semiconductors* (U.S. AEC, Oak Ridge, Tenn., 1970), p. 439.
[10]G. W. Gobeli and E. O. Kane, Phys. Rev. Lett. 15, 142 (1965); B. O. Seraphin, Phys. Rev. 140, 1716 (1965); B. O. Seraphin and N. Bottka, *ibid.* 145, 628 (1966); A. K. Ghosh, Phys. Lett. 23, 36 (1966); M. Cardona, K. L. Shaklee, and F. H. Pollak, Phys. Rev. 154, 696 (1967); A. Balzarotti and M. Grandolfo, Solid State Commun. 6, 815 (1968); E. Matatagui, A. G. Thompson, and M. Cardona, Phys. Rev. 176, 950 (1968); F. H. Pollak and M. Cardona, *ibid.* 172, 816 (1968); J. Koo, Y. R. Shen, and R. R. L. Zucca, Solid State Commun. 9, 2229 (1971); F. H. Pollak and G. W. Rubloff, Phys. Rev. Lett. 29, 789 (1972); S. S. Vishnubhatla and V. Makios, Phys. Lett. A 40, 221 (1972); M. Welkowsky and R. Braunstein, Phys. Rev. B 5, 497 (1972).
[11]R. A. Forman, D. E. Aspnes, and M. Cardona, J. Phys. Chem. Solids 31, 227 (1970).
[12]D. E. Aspnes and A. A. Studna, Solid State Commun. 11, 1375 (1972).
[13]J. W. Grover and P. Handler, Phys. Rev. B 9, 2600 (1974).
[14]K. Kondo, A. Moritani, C. Hamaguchi, and J. Nakai, Solid State Commun. 15, 1525 (1974).
[15]K. Kondo and A. Moritani, Phys. Rev. B 14, 1577 (1976).
[16]K. Kondo and A. Moritani, Phys. Rev. B 15, 812 (1977).
[17]D. Brust, M. L. Cohen, and J. C. Phillips, Phys. Rev. Lett. 9, 389 (1962); D. Brust, Phys. Rev. 134, A1337 (1964); 139, A489 (1965); M. L. Cohen and T. K. Bergstresser, *ibid.* 141, 789 (1966).
[18]M. Cardona and F. H. Pollak, Phys. Rev. 142, 530 (1966).
[19]F. Herman, R. L. Kortum, C. D. Kuglin, and R. A. Short, in *Quantum Theory of Atoms*, edited by P. O. Löwdin (Academic, New York, 1966), p. 381.
[20]E. O. Kane, Phys. Rev. 146, 558 (1966).
[21]L. R. Saravia and D. Brust, Phys. Rev. 171, 916 (1968).
[22]L. R. Saravia, J. Phys. Chem. Solids 35, 1469 (1974).
[23]J. R. Chelikowsky and M. L. Cohen, Phys. Rev. B 10, 5095 (1974).
[24]M. Cardona and D. L. Greenaway, Phys. Rev. 125, 1291 (1962).
[25]M. Cardona, Phys. Rev. B 15, 5999 (1977).
[26]E. O. Kane, Phys. Rev. 175, 1039 (1968).
[27]S. Zwerdling, K. J. Button, B. Lax, and L. M. Roth, Phys. Rev. Lett. 4, 173 (1960).
[28]D. E. Aspnes, Opt. Commun. 8, 222 (1973); D. E. Aspnes and A. A. Studna, Appl. Opt. 14, 220 (1975).
[29]P. S. Hauge and F. H. Dill, IBM J. Res. Devel. 17, 472 (1973).
[30]D. E. Aspnes, in *Proceedings of the Twelfth International Conference on the Physics of Semiconductors* (Teubner, Stuttgart, 1974), p. 1197.
[31]R. W. G. Wyckoff, *Crystal Structures* (Wiley-Interscience, New York, 1963), Vol. 1.
[32]D. E. Aspnes, Phys. Rev. B 12, 2297 (1975).
[33]E. O. Kane, Phys. Rev. 180, 852 (1969).
[34]D. F. Blossey, Phys. Rev. B 2, 3976 (1970); 3, 1382 (1971).
[35]F. C. Weinstein, J. D. Dow, and B. Y. Lao, Phys. Rev. B 4, 3502 (1971).
[36]D. E. Aspnes, Phys. Rev. Lett. 31, 230 (1974).
[37]D. E. Aspnes and J. E. Rowe, Phys. Rev. Lett. 27, 188 (1971).
[38]D. E. Aspnes, P. Handler, and D. F. Blossey, Phys. Rev. 166, 921 (1968).
[39]D. E. Aspnes and J. E. Rowe, in Ref. 9, p. 422.
[40]D. E. Aspnes and A. Frova, Solid State Commun. 7, 155 (1969).
[41]A. R. Reinberg, Appl. Opt. 11, 1273 (1972); S. S. So and K. Vedam, J. Opt. Soc. Am. 62, 16 (1972); D. E. Aspnes, in Ref. 1d, p. 801.
[42]D. E. Aspnes, J. Opt. Soc. Am. 64, 812 (1974).
[43]Model LT-3, manufactured by Air Products and Chemicals, Inc., Allentown, Pa 18105.
[44]J. C. Phillips, Solid State Phys. 18, 55 (1966); Y. Toyozawa, M. Inoue, T. Inui, M. Okazaki, and E. Hanamura, J. Phys. Soc. Jpn. 21, 208 (1968); B. Velicky and J. Sak, Phys. Status Solidi 16, 147 (1966).
[45]D. Auvergne, J. Camassel, H. Mathieu, and M. Cardona, Phys. Rev. B 9, 5168 (1974).
[46]D. E. Aspnes, C. G. Olson, and D. W. Lynch, Phys. Rev. B 14, 4450 (1976).
[47]S. Koeppen, P. Handler, and S. Jasperson, Phys. Rev. Lett. 27, 265 (1971).
[48]K. C. Pandey and J. C. Phillips, Phys. Rev. B 9, 1551 (1974).
[49]J. S. Kline, F. H. Pollak, and M. Cardona, Helv. Phys. Acta 41, 968 (1968).